SUPPORTING INFORMATION

A Rare Example of a Krypton Difluoride Coordination Compound; $[BrOF_2][AsF_6]\cdot 2KrF_2$

David S. Brock,[†] Jonathan J. Casalis de Pury,[†] Hélène P. A. Mercier,[†]

Gary J. Schrobilgen,[†] and Bernard Silvi[‡]

[†] Department of Chemistry, McMaster University, Hamilton, Ontario, L8S 4M1, Canada

[‡] Laboratoire de Chimie Théorique (UMR-CNRS 7616), Université Pierre et Marie Curie-Paris 06, 4, place Jussieu, 75252 Paris cédex, France

Complementary Discussion of the X-ray Crystal Structure of $[BrOF_2][AsF_6]\cdot 2KrF_2$.

The NBO analysis (PBE1PBE and B3LYP values are taken from Table S3 ; B3LYP values are in parentheses) assigns a bond order of 0.10 (0.08) for Br---F compared to 0.50 (0.39) for the Br–F bond of the $BrOF_2^+$ cation in the complex and 0.38 (0.37) for the terminal and 0.25 (0.24) for the bridge Kr–F bonds of the coordinated KrF_2 molecules. Because the lone pair-bond pair repulsions are less for these long and very ionic bridge bonds, the angles will be significantly more open than the ideal tetrahedral angle of an AX_2E_2 VSEPR arrangement. Similar reasoning applies to the Br(1)---F(7)–As(1) angle where the Br---F and As–F bond orders are 0.04 (0.04) and 0.47 (0.46), respectively.

Table S1. Factor-Group Analysis for $[BrOF_2][AsF_6]\cdot 2KrF_2$

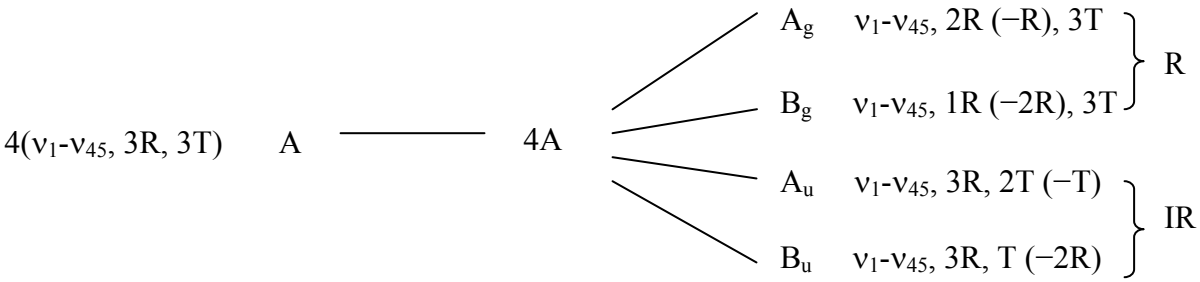

[a] The crystallographic space group is $P2_1/c$ with $Z = 4$ structural units per unit cell.

Table S2. Experimental and Calculated Frequencies[a] for KrF_2

exptl	PBE1PBE[b]	B3LYP[b]	assgnts[c]
580[d]	613(<1)[287]	584(<0.1)[260]	$\nu_3(\Sigma_u^-)$ $\nu_{as}(KrF_2)$
465.5[e]	526(51)[<1]	493(52)[<0.1)	$\nu_1(\Sigma_g^+)$ $\nu_s(KrF_2)$
469.5, 468.6[f]			
236 [d]	249(<0.1)[14]	234(<0.1)[13]	$\nu_2(\Delta_u)$ $\delta(KrF_2)$

[a] Frequencies are given in cm^{-1}. [b] The aug-cc-pVTZ(-PP) basis set was used. Values in parentheses denote Raman intensities ($Å^4$ u^{-1}). Values in square brackets denote infrared intensities (km mol^{-1}). [c] The abbreviations denote symmetric (s), asymmetric (as), stretch (ν) and bend (δ). [d] Infrared values obtained from matrix-isolated KrF_2 in ref 39. [e] Raman frequencies for the α-phase of KrF_2 are from ref 36. [f] Raman frequencies for the β-phase of KrF_2 are from ref 36.

Table S3. NBO Valencies, Bond Orders, and Charges (NPA) for $BrOF_2^+$, $[BrOF_2][AsF_6]\cdot 2KrF_2$, and KrF_2

	$BrOF_2^+$				$[BrOF_2][AsF_6]\cdot 2KrF_2$				KrF_2			
Charges [Valencies]												
	PBE1PBE		B3LYP		PBE1PBE		B3LYP		PBE1PBE		B3LYP	
Br(1)	2.326	[1.325]	2.298	[1.294]	2.411	[2.270]	2.381	[1.893]				
O(1)	-0.586	[0.594]	-0.563	[0.602]	−0.715	[0.953]	−0.695	[0.843]				
F(1)	-0.370	[0.271]	-0.368	[0.257]	−0.446	[0.457]	−0.445	[0.357]				
F(2)	-0.370	[0.271]	-0.368	[0.257]	−0.445	[0.455]	−0.446	[0.355]				
Kr(1)					1.081	[0.645]	1.065	[0.619]	1.032	[0.619]	1.013	[0.588]
F(3)					−0.579	[0.351]	−0.570	[0.326]	−0.516	[0.326]	−0.506	[0.309]
F(4)					−0.432	[0.394]	−0.420	[0.378]	−0.516	[0.326]	−0.506	[0.309]
Kr(2)					1.084	[0.667]	1.065	[0.635]	1.032	[0.619]	1.013	[0.588]
F(5)					−0.576	[0.372]	−0.566	[0.341]	−0.516	[0.326]	−0.506	[0.309]
F(6)					−0.422	[0.404]	−0.414	[0.380]	−0.516	[0.326]	−0.506	[0.309]
As(1)					2.638	[3.222]	2.640	[3.152]				
F(7)					−0.634	[0.464]	−0.636	[0.443]				
F(8)					−0.573	[0.502]	−0.571	[0.490]				
F(9)					−0.612	[0.466]	−0.606	[0.460]				
F(10)					−0.589	[0.490]	−0.593	[0.473]				
F(11)					−0.566	[0.506]	−0.565	[0.492]				
F(12)					−0.626	[0.467]	−0.623	[0.447]				
Bond Orders												
Br(1)-O(1)	0.670		0.674		1.023		0.905					
Br(1)-F(1)	0.328		0.310		0.493		0.389					
Br(1)-F(2)	0.328		0.310		0.497		0.391					
Br(1)---F(3)					0.092		0.075					
Br(1)---F(5)					0.103		0.081					
Br(1)---F(7)					0.042		0.041					
Kr(1)-F(3)					0.244		0.234		0.310		0.294	
Kr(1)-F(4)					0.380		0.365		0.310		0.294	
Kr(2)-F(5)					0.250		0.241		0.310		0.294	
Kr(2)-F(6)					0.389		0.368		0.310		0.294	
As(1)-F(7)					0.474		0.455					
As(1)-F(8)					0.574		0.564					
As(1)-F(9)					0.530		0.526					
As(1)-F(10)					0.555		0.539					
As(1)-F(11)					0.580		0.567					
As(1)-F(12)					0.508		0.502					

Outline of QTAIM and ELF. The QTAIM analysis provides a partition into atomic basins over which it is possible to integrate densities of properties in order to obtain atomic properties such as atomic populations, $\bar{N}(\mathrm{A})$. In the QTAIM framework, bonded atoms are linked by a bond path[S1,S2] which is defined as the union of the trajectories joining the bond critical point (bcp), a saddle point maximum in two directions located on the border surface of two atomic basins, to the two nuclei. The value of the Laplacian of the density at the bond critical point, as well as those of other functions, is used to further characterize the interaction: a negative value of $\nabla^2\rho(\mathrm{r}_{bcp})$ corresponds to a shared-electron (covalent) interaction whereas a positive value indicates an unshared-electron bonding mode. Moreover, insights into the delocalization in terms of delocalization indices[S3] can be obtained by a covariance analysis of the atomic populations.

The electron localization function, denoted $\eta(\mathbf{r})$, was originally conceived as a local measure of the Fermi hole curvature around a reference point within the Hartree-Fock approximation.[S4] A further interpretation, in terms of a local excess of kinetic energy due to the Pauli principle, was proposed by Savin et al.,[S5] which legitimatized the calculation of the function with Kohn-Sham orbitals. More recently, it was shown that the ELF kernel can be rigorously derived by considering the same number of spin pairs contained in a sample around the reference point.[S6,S7] A cosmetic Lorentz transform that confines the ELF is the [0,1] interval; where 1 corresponds to regions dominated by an opposite spin pair or by a single electron, whereas low values are found at the boundaries between such regions. The basins of ELF attractors are closely related to Gillespie's electronic domains and recover the ideas of Lewis. There are two types of basins: core basins, denoted by C(A), encompassing the nucleus of atom A and valence basins, denoted by V(A, B, …). The valence shell of an atom, say A, in a molecule is therefore the union of valence basins having a boundary with C(A). A valence basin may belong to several atomic valence shells. The synaptic order[S8] is defined as the number of such valence shells which a valence basin participates in. There are therefore monosynaptic basins, V(A), corresponding to the lone pair, disynaptic basins V(A, B) corresponding to two center bonds, and higher polysynaptic basins for polycentric bonds. The basin populations and the associated covariance matrix are calculated by integration of the one electron and pair densities over the volumes of the basins, enabling a phenomenological interpretation of the population analysis in terms of the superposition of mesomeric structures.[S9] The weights of these structures are estimated from the populations, the covariance matrices, and for the probabilities of finding N electrons in a given basin.[S10,S11] The concept of localization domain[S12] has been introduced for graphical purposes and to also define a hierarchy of the localization basins which can be related to chemical properties. A localization domain is a volume limited by one or more closed isosurfaces denoted by $\eta(\mathbf{r}) = f$, where f is defined as the isosurface contour. A localization domain surrounds at least one attractor- in this case it is called irreducible. If the delocalization domain contains more than one attractor, it is termed reducible. Except for atoms and linear molecules, the irreducible domains are always filled volumes whereas the reducible domains can be either filled volumes, hollow volumes, or tori. Upon increasing the value of $\eta(\mathbf{r})$, which defines the boundary isosurface, a reducible domain splits into several domains, each containing less attractors than the parent one. The reduction of localization occurs at the turning points which are critical points of index 1 located on the separatrix of two basins involved in the parent domain. Ordering these turning points (localization nodes) by increasing $\eta(\mathbf{r})$ enables one to build tree-diagrams reflecting the hierarchies of the basins.[S13,S14]

The QTAIM approach provides a phenomenological representation of the molecular electron density, and therefore of the bonding, close to the superposition of promolecular atomic

densities, whereas ELF intends to recover the VSEPR and Lewis pictures. An interesting combination of QTAIM and ELF has been proposed by Raub and Jansen[S15] who considered the contributions of the atomic basins to the ELF valence basin populations. As a general rule, the number of contributing atomic basins is equal to the synaptic order. Indeed, the QTAIM and ELF analysis are almost equivalent in unshared-electron systems.

(i) Nature of the Bonding in KrF_2. In order to understand the nature of the Kr−F interaction in KrF_2, the KrF molecule was first considered. The ground state of KrF is a $^2\Sigma$ doublet, with an optimized internuclear distance of 2.437 and 2.410 Å using the PBE1PBE and B3LYP hybrid functionals. The calculated binding energy is rather weak; 10 kJ mol^{-1} with PBE1PBE and 16 kJ mol^{-1} with B3LYP. The AIM analysis provided the following information: (1) the atomic populations indicate a significant charge transfer of 0.15 e towards the fluorine atom, this value coincides with the NBA net positive charges of the KrF_2 ligands (0.19 and 0.09) (Table S3), (2) the spin density is mostly in the F basin (85%), (3) the delocalization index, $\delta = 0.42$, is typical of a weak interaction; β-spin electrons contribute three times more than the α-spin electrons to this index, (4) the density value at the bond critical point is small, $\rho(r_{bcp}) = 0.036$ e $bohr^{-3}$, and its Laplacian is positive ($\nabla^2\rho(r_{bcp}) = 0.157$ e $bohr^{-5}$).

The bonding is therefore characterized by a charge transfer and a small delocalization of the single electron over the two atoms. The QTAIM population analysis suggests a picture of the bonding represented by the following superposition of two promolecular densities:

Kr F↑ 85%

Kr^+↑ F 15%

The ELF reduction of the localization diagram of KrF (Scheme S1) shows that the Kr and F atoms can be considered as two independent interacting chemical systems because the separation of V(F) from V(Kr) occurs at almost the same value as the fluorine core-valence bifurcation. The population analysis is consistent with this picture and confirms the conclusions drawn from the QTAIM results: there is no disynaptic basin and the values of the basin populations, integrated spin densities, and covariance matrix elements are in complete agreement with those of QTAIM.

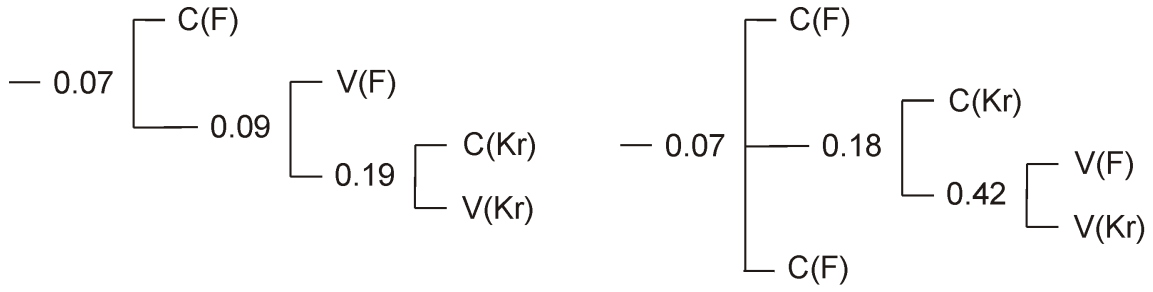

Scheme S1. Reduction of the localization diagrams for KrF (left) and KrF_2 (right) showing the ordering of localization nodes and the boundary isosurface value, $\eta(\mathbf{r})$, at which the reducible domains split.

The ground state of KrF_2 is a singlet $^1\Sigma_g$; the Kr−F internuclear distances are significantly shorter than in KrF, 1.860 and 1.890 Å, at the PBE1PBE and B3LYP levels, respectively, and the binding energy per fluorine is much larger; 58 (PBE1PBE) and 63 mol^{-1} (B3LYP). The atomic populations of Kr and F indicate a net density transfer of 0.48 e from Kr to each F, in good agreement with the NBO analysis which yields 0.52 e. The Kr−F and F−F delocalization indexes are 0.86 and 0.22, respectively. Finally, the Laplacian of the density at the KrF bond critical point is positive ($\nabla^2\rho(r_{bcp}) = 0.23$ e $bohr^{-5}$). The ELF reduction of localization diagram of KrF_2, Scheme S1, which is at variance with KrF, shows that the separation of the molecular valence shell into its atomic components occurs at a larger ELF value than the Kr core-valence separation. Therefore, KrF_2 can be considered as a single chemical entity rather than as a cluster of interacting atoms. Figure S1 displays the ELF localization domains for KrF_2 at $\eta(\mathbf{r}) = 0.75$, showing the absence of any disynaptic (bond) between Kr and F. The ELF population analysis, reported in Table S4, together with the QTAIM results suggests an interpretation of the bonding in terms of a large delocalization of the electron density between the Kr and F valence shells and of an electron density transfer towards the fluorine atom. This type of bonding looks very similar to the charge-shift bonds introduced by Shaik et al.,[S16−4S18] but there are some important differences. If the Kr−F bond was a standard charge-shift bond, it should have almost the same properties in KrF and KrF_2. Comparison of the two molecules shows a cooperative effect that enhances the bond strength in KrF_2. The main difference between the ground states of these molecules is that KrF is a doublet and KrF_2 a singlet, therefore the addition of a second fluorine atom removes the spin density that is mostly localized on the first fluorine. Because there is no direct interaction between the two fluorine atoms, there is mediation on the part of the Kr atom which plays a role very similar to that of the non-magnetic anion in superexchange coupling. Weighted promolecular mesomeric forms can be proposed from the probabilities of finding *n* electrons in a given basin (Scheme S2).

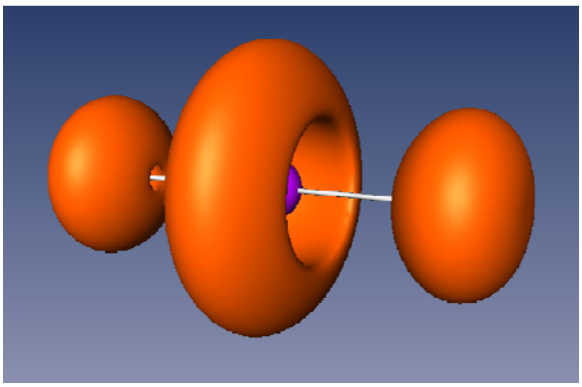

Figure S1. ELF localization domains of KrF_2. The isosurface value is $\eta(\mathbf{r}) = 0.75$. Color code: magenta = core, brick-red = monosynaptic basin.

The spacial symmetry and the diamagnetism of KrF_2 explain the multiplicity of each kind of structure. This multiplicity and the large increase in weighting of the ionic structures with respect to KrF contribute to the stabilization of the molecule.

Table S4. ELF Basin Population and Covariance Matrix Elements of KrF_2

	aug-cc-pVTZ		DGDZVP
	B3LYP	PBE1PBE	PBE1PB
$\bar{N}$ [C(F)]	2.11	2.16	2.13
$\bar{N}$ [C(Kr)] [a]	17.88	17.89	27.72
$\bar{N}$ [V(F)]	7.31	7.30	7.30
$\bar{N}$ [V(Kr)]	7.25	7.17	7.41
$\langle cov[V(Kr),V(F)]\rangle$	−0.41	−0.42	−0.40
$\langle cov[V(F),V(F')]\rangle$	−0.9	−0.8	−0.08

[a] The use of pseudo-potential calculations and the all electron calculation account for the differences in the Kr basin populations.

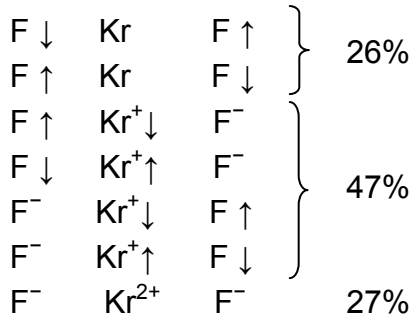

Scheme S2. Weighted promolecular mesomeric forms of KrF_2 and their probabilities.

(ii) Nature of the Bonding in $BrOF_2^+$. The $BrOF_2^+$ cation has a trigonal pyramidal geometry according to the VSEPR rules. Because all atoms have lone pairs, the lone-pair bond weakening effect (LPBWE)[S19] is expected to be important. The QTAIM electronic populations localize a large positive charge (+2.25) on bromine and partial negative charges on the oxygen (−0.52) and fluorine (−0.36) atoms. These values are in good agreement with the NPA charges +2.30, −0.57, and −0.36 for Br, O and F, respectively. The delocalization indexes (δ) indicate delocalization between the Br and O basins (δ = 1.84) that is twice that of Br and F (δ = 0.98) as well as rather important interactions between non-bonded atoms such as between O and F (δ = 0.24), and between the two fluorines (δ = 0.12). The values of the Laplacian of the electron density are both positive at the Br−O and Br−F bond critical points (0.39 and 0.29, respectively). Therefore, the bonding can be described as belonging to the unshared-electron type.

Figure 5 displays the localization domains of $BrOF_2^+$ which either belong to core or to monosynaptic valence basins at $\eta(\mathbf{r})$ = 0.75. The reduction of localization diagram (Scheme S3) indicates, however, that there is only one valence shell because the core valence separations occur at ELF values lower than the division of the valence density. While the atomic valence shells of O and F can be easily identified, each of them being the union of two monosynaptic basins, only V(Br) can be unambiguously assigned to the Br valence shell. In the ELF population

analysis presented in Table S5, the two V(O) basins as well as the V(F) basins of each fluorine have merged into single basins. The population of the V(Br) basin, 3.11 e, is larger than expected for a single lone pair, and is a consequence of the LPBWE which tends to increase the lone pair population at the expense of bonding. The covariance matrix elements between V(Br) and the other valence basins are very large although these basins belong, in principle, to different atomic valence shells. The large contributions of the Br atomic basin to V(O) and to V(F), however, suggest participation of these basins in the Br valence shell. In particular, $\bar{N}$ [V(O)|Br] = 1.5 e, is consistent with a dative picture of the Br−O bond.

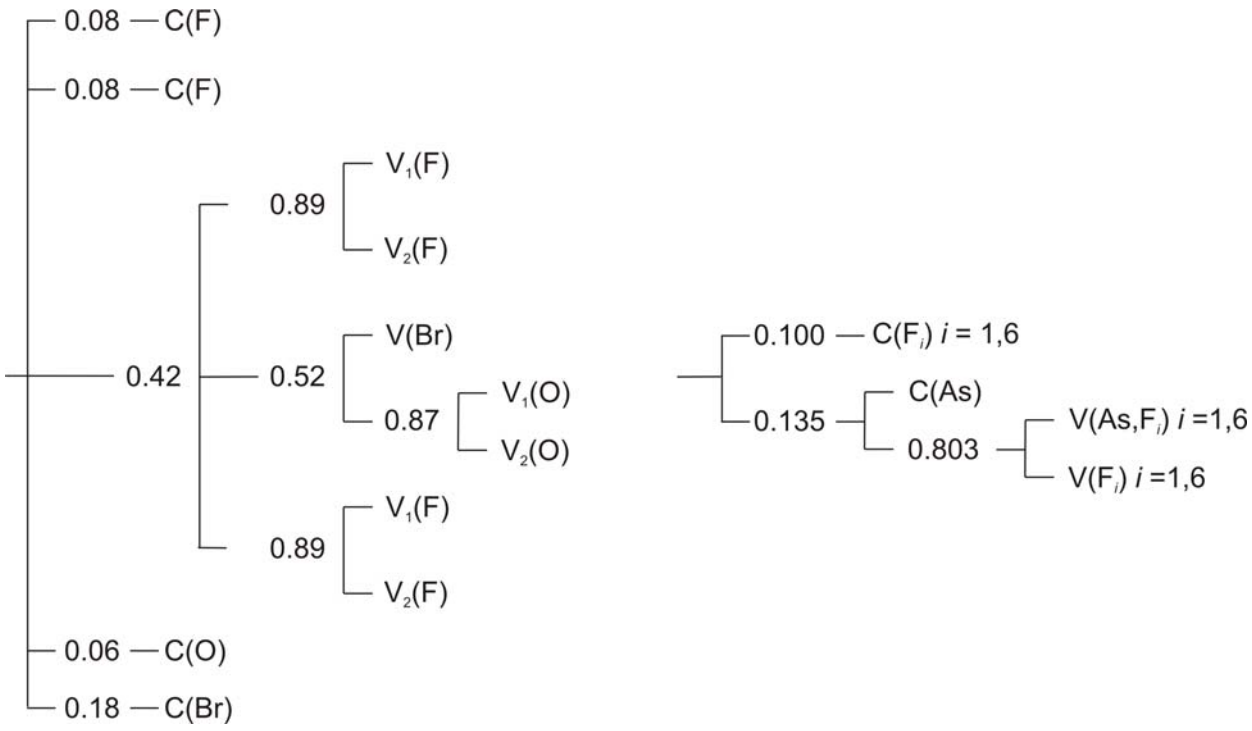

Scheme S3. Reduction of localization diagrams for $BrOF_2^+$ (left) and AsF_6^- (right) showing the ordering of localization nodes and the boundary isosurface values, $\eta(\mathbf{r})$, at which the reducible domains split.

(iii) Nature of the Bonding in AsF_6^-. Both QTAIM and ELF describe the bonding in the AsF_6^- anion as arising from both ionic and covalent resonance structures. Charge-shift bonding is not possible in this system because there is no lone pair on the As atom. From the QTAIM point of view, the large positive value of the Laplacian of the charge density at the As−F bond critical point, 0.613, is indicative of a dominant unshared-electron interaction whereas the fluorine net charge, −0.67 e, indicates that the weights of the contributing mesomeric structures involving covalent As−F are rather large. The ELF analysis confirms this picture because there are six V(As,F) disynaptic basins displayed in Figure S2. Although the population of this basin is very

low, 0.16 e, the total contribution of the atomic As basin to the V(F) basins amounts to 1.26 e. Accordingly, the dominant resonance structures should be: $AsF^{4+}(F^{-})_5$ (~31%), $AsF_2^{3+}(F^{-})_4$ (~34%), and $AsF_3^{2+}(F^{-})_3$ (~25%).

Table S5. ELF Basin Population, $\bar{N}[\Omega]$, Covariance Matrix Elements, $\langle cov(\bar{N}[\Omega], \bar{N}[\Omega'])\rangle$, and Bromine Atomic Basin Contribution, ($\bar{N}[\Omega|Br]$), of $BrOF_2^+$

Ω	$\bar{N}[\Omega]$	$\langle cov(\bar{N}[\Omega], \bar{N}[\Omega'])\rangle$				$\bar{N}[\Omega\|Br]$
		V(F)	V(O)	V(Br)	V(F')	
V(F)	7.45	1.07	−0.09	−0.26	−0.08	0.25
V(O)	7.91	−0.09	1.68	−0.45	−0.09	1.5
V(Br)	3.11	−0.26	−0.45	1.64	−0.26	3.11

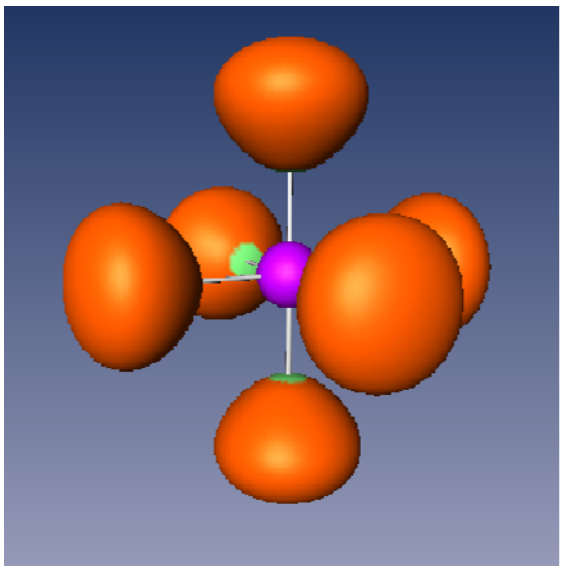

Figure S2. ELF localization domains for AsF_6^-. The isosurface value is $\eta(\mathbf{r}) = 0.75$. Color code: magenta = core, brick-red = monosynaptic basin, green = disynaptic basin.

(S1) Runtz, G. R.; Bader, R. F. W.; Messer, R. R. *Can. J. Chem.* **1977**, *55*, 3040–3045.
(S2) Bader, R. F. W. *J. Phys. Chem. A* **1998**, *102*, 7314−7323.
(S3) Fradera, X.; Austen, M. A.; Bader, R. F. W. *J. Phys. Chem. A* **1998**, *103*, 304–314.
(S4) Becke, A. D.; Edgecombe, K. E. *J. Chem. Phys.* **1990**, *92*, 5397–5403.
(S5) Savin, A.; Becke, A. D.; Flad, J.; Nesper, R.; Preuss, H.; von Schnering, H. G. *Angew. Chem. Int. Ed. Engl.* **1991**, *30*, 409−412.
(S6) Silvi, B. *J. Phys. Chem. A* **2003**, *107*, 3081–3085.
(S7) Kohout, M.; Pernal, K.; Wagner, F. R.; Grin, Y. *Theor. Chem. Acc.* **2004**, *112*, 453–459.

(S8) Silvi, B. *J. Mol. Struct.* **2002**, *614*, 3–10.
(S9) Silvi, B. *Phys. Chem. Chem. Phys.* **2004**, *6*, 256–260.
(S10) Bader, R. F. W.; Stephens, M. E. *Chem. Phys. Lett.* **1974**, *26*, 445−449.
(S11) Cances, E.; Keriven, R.; Lodier, F.; Savin, A. *Theor. Chem. Acc.* **2004**, *111*, 373–380.
(S12) Silvi, B.; Savin, A. *Nature* **1994**, *371*, 683–686.
(S13) Savin, A.; Silvi, B.; Colonna, F. *Can. J. Chem.* **1996**, *74*, 1088–1096.
(S14) Calatayud, M.; Andrés, J.; Beltrán, A.; Silvi, B. *Theor. Chem. Acc.* **2001**, *105*, 299–308.
(S15) Raub, S.; Jansen, G. *Theor. Chem. Acc.* **2001**, *106*, 223–232.
(S16) Shaik, S.; Maitre, P.; Sini, G.; Hiberty, P. C. *J. Am. Chem. Soc.* **1992**, *114*, 7861–7866.
(S17) Shaik, S.; Danovich, D.; Silvi, B.; Lauvergnat, D.; Hiberty, P. *Chem. Eur. J.* **2005**, *21*, 6358–6371.
(S18) Shaik, S.; Danovich, D.; Wu, W.; Hiberty, P. *Nature Chemistry* **2009**, *1*, 443–449.
(S19) Sanderson, R. T. *Polar Covalence*. Academic Press: New York, NY, 1983.

Complete reference 59. Frisch, M. J.; Trucks, G. W.; Schlegel, H. B.; Scuseria, G. E.; Robb, M. A.; Cheeseman, J. R.; Zakrzewski, V. G.; Montgomery, J. A., Jr.; Stratmann, R. E.; Burant, J. C.; Dapprich, S.; Millam, J. M.; Daniels, A. D.; Kudin, K. N.; Strain, M. C.; Farkas, O.; Tomasi, J.; Barone, V.; Cossi, M.; Cammi, R.; Mennucci, B.; Pomelli, C.; Adamo, C.; Clifford, S.; Ochterski, J.; Petersson, G. A.; Ayala, P. Y.; Cui, Q.; Morokuma, K.; Salvador, P.; Dannenberg, J. J.; Malick, D. K.; Rabuck, A. D.; Raghavachari, K.; Foresman, J. B.; Cioslowski, J.; Ortiz, J. V.; Baboul, A. G.; Stefanov, B. B.; Liu, G.; Liashenko, A.; Piskorz, P.; Komaromi, I.; Gomperts, R.; Martin, R. L.; Fox, D. J.; Keith, T.; Al-Laham, M. A.; Peng, C. Y.; Nanayakkara, A.; Challacombe, M.; Gill, P. M. W.; Johnson, B.; Chen, W.; Wong, M. W.; Andres, J. L.; Gonzalez, C.; Head-Gordon, M.; Replogle, E. S.; Pople, J. A.; *Gaussian 98*, Revision A.11; Gaussian, Inc.: Pittsburgh, PA, 2003.